

Using 2D In Vivo IVUS-Based Models for Human Coronary Plaque Progression Analysis and Comparison with 3D Fluid-Structure Interaction Models: A Multi-Patient Study

Hongjian Wang^{*}, Jie Zheng[†], Liang Wang[‡], Akiko Maehara[§], Chun Yang[¶], David Muccigrosso[†], Richard Bach^{||}, Jian Zhu^{**}, Gary S. Mintz[§] and Dalin Tang^{*,‡,††}

Abstract: Computational modeling has been used extensively in cardiovascular and biological research, providing valuable information. However, 3D vulnerable plaque model construction with complex geometrical features and multi-components is often very time consuming and not practical for clinical implementation. This paper investigated if 2D atherosclerotic plaque models could be used to replace 3D models to perform correlation analysis and achieve similar results. In vivo intravascular ultrasound (IVUS) coronary plaque data were acquired from a patient follow-up study to construct 2D structure-only and 3D FSI models to obtain plaque wall stress (PWS) and strain (PWSn) data. One hundred and twenty-seven (127) matched IVUS slices at baseline and follow up were obtained from 3 patients. Our results showed that 2D models overestimated stress and strain by 30% and 33%, respectively, compared to results from 3D FSI models. 2D/3D correlation comparison indicated that 116 out of 127 slices had a consistent correlation between plaque progression (WTI) and wall thickness; 103 out of 127 slices had a consistent correlation between WTI and PWS; and 99 out of 127 slices had a consistent correlation between WTI and PWSn. This leads to the potential that 2D models could be used in actual clinical implementation where quick analysis

^{*} School of Biological Science and Medical Engineering, Southeast University, Nanjing, 210096, China.

[†] Mallinckrodt Institute of Radiology, Washington University, St. Louis, MO, USA.

[‡] Mathematical Sciences Department, Worcester Polytechnic Institute, MA, USA.

[§] The Cardiovascular Research Foundation, NY, NY, USA.

[¶] Network Technology Research Institute, China United Network Communications Co., Ltd., Beijing, China.

^{||} Cardiovascular Division, Washington University School of Medicine, Saint Louis, MO, USA.

^{**} Department of Cardiology, Zhongda Hospital, Southeast University, Nanjing, China.

^{††} Corresponding author. Tel: 508-845-1575; E-mail: dtang@wpi.edu

delivery time is essential.

Keywords: Coronary, 2D structure-only, fluid-structure interaction, plaque rupture, plaque progression, IVUS.

1 Introduction

It is believed that atherosclerotic plaque progression is related to multiple factors including morphological factors, plaque tissue components, material properties, and mechanical stress and strain conditions [1-6]. Considerable progress in medical imaging and image-based plaque models have been made in determining plaque morphology, components, fibrous cap, lipid-rich necrotic core, plaque stress, strain and flow shear stress conditions [2,7]. However, mechanisms governing plaque progression and causing plaque rupture are not well understood [1,2,6]. By using in vivo human carotid MRI data, Tang et al. indicated that plaque progression correlated negatively with plaque wall stress [8]. In a prediction study of progression of coronary disease, 506 patients with acute coronary syndrome (ACS) treated with a percutaneous coronary intervention and in a subset of 374 consecutive patients 6-10 months later to assess plaque natural history, Stone et al. reported that large plaque burden and low local wall shear stress provide independent and additive prediction to identify plaques that develop progressive enlargement and lumen narrowing [9]. In a follow up study of 20 patients with coronary artery disease, Samady et al. found that low-WSS segments develop greater plaque and necrotic core progression and constrictive remodeling, and high-WSS segments develop greater necrotic core and calcium progression, regression of fibrous and fibrofatty tissue, and excessive expansive remodeling, suggestive of transformation to a more vulnerable phenotype [10]. In the PROSPECT study (660 patients with complete IVUS data), Xie et al. [11] reported that the current 3-vessel IVUS analysis of 660 patients in the PROSPECT study showed that the prevalence of secondary, nonculprit plaque ruptures in patients with ACS was 14.1%, that it was associated with a VH fibroatheroma phenotype with a residual necrotic core in three-fourths of patients and a VH-TCFA phenotype with a residual necrotic core in approximately one-half of patients, and that it was not associated with subsequent MACE in patients treated with proper medical therapy. Yang et al. [12] reported that advanced carotid plaque progression had positive correlation with wall shear stress (WSS) and negative correlation with plaque wall stress (PWS) at follow-up. We have published results based on follow up study, by constructing 3D FSI models, showing that a combination of wall thickness and plaque wall stress was identified as the best predictor for plaque progression measured by WTI [13]. Huang et al. [14] reported that compared to 3D fully coupled FSI models, 2D structure-only simulation significantly

overestimated stress level (94.1kPa [65.2, 117.3] vs. 85.5kPa [64.4, 113.6]; median [inter-quartile range], $p=0.0004$). However, when slices around the bifurcation region were excluded, stresses predicted by 2D structure-only simulations showed a good correlation ($R^2 = 0.69$) with values obtained from 3D fully coupled FSI analysis.

In this paper, intravascular ultrasound (IVUS) patient follow-up data were acquired and IVUS-based 2D structure-only models and 3D fluid-structure interactions (FSI) with cyclic bending were respectively constructed to obtain plaque morphological features, plaque wall stress/strain data and identify their possible associations with plaque progression measured by wall thickness increase. Correlations result comparisons between 2D structure-only and 3D FSI models were presented. The purpose of this study was to see if 2D models could be used to replace 3D models to perform correlation analysis and achieve similar results for plaque progression study.

2 Methods

2.1 IVUS Data Acquisition and Registration

Patient follow-up IVUS data of coronary plaques were acquired from 3 patients (3M, age: 52/71/68) at Cardiovascular Research Foundation (New York, NY) after informed consent was obtained, using established procedures described in Yang et al. [15]. Patient information are given in Table 1. Vessel and multi-components detection was performed to obtain IVUS-VH (Virtual Histology) data using automated Virtual Histology software (version 3.1) on a Volcano s5 Imaging System (Volcano Crop., Rancho Cordova, CA). IVUS-VH slices at the baseline (T1) and follow-up (T2) were processed to obtain contours for vessel lumen, out-boundary and plaque components for model construction. X-ray angiogram (Allura Xper FD10 System, Philips, Bothel, WA) was obtained prior to the pullback of the IVUS catheter to determine the location of the coronary artery stenosis and vessel curvature variations. Fusion of angiography and IVUS slices was done using method similar to that described in Wahle et al. [16] except that we did not have biplane angiography. The view angle of the angiography was chosen so that the angiography plane was close to the principal tangent plane of the chosen coronary segment. Co-registration (both longitudinal and circumferential) of baseline and follow-up IVUS data were performed by IVUS expert using angiography movie, location of the myocardium, vessel bifurcation, stenosis and plaque component features. The location of the myocardium was used in circumferential co-registration. Figure 1 presents matched selected IVUS-VH slices from one patient at T1 and T2, the corresponding segmented contours, enlarged view of one slice, and the reconstructed

3D geometry of the plaque at T1. The X-ray angiogram and vessel bending curves with minimum curvature were shown by Figure 2.

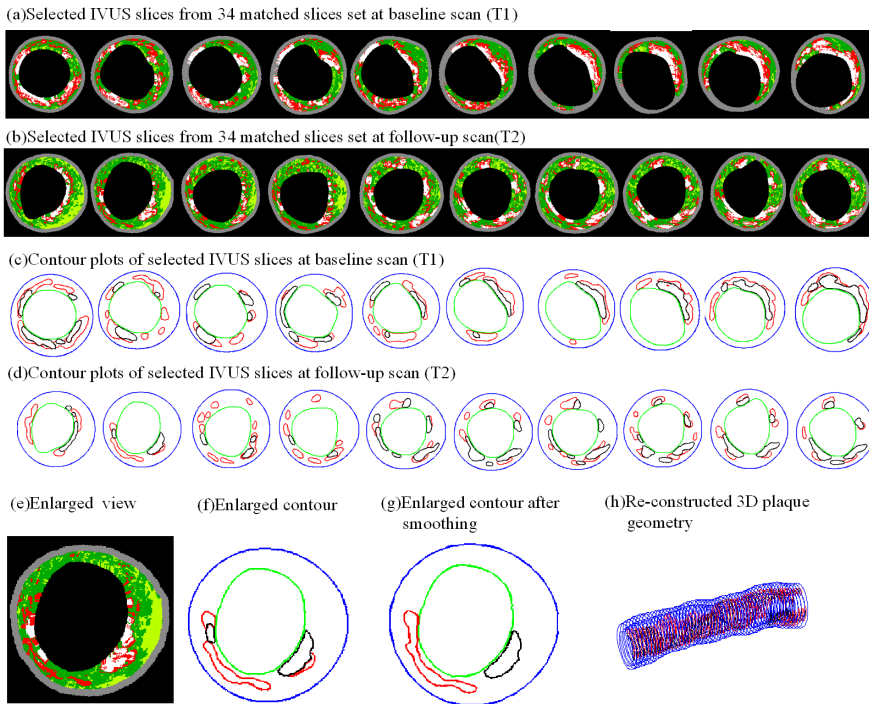


Figure 1: Matched IVUS-VH and segmented contour plots of slices from baseline (T1) and follow-up (T2). Plots also include enlarged view of a slice, and re-constructed 3D plaque geometry. Colors used in IVUS-VH: Red-necrotic core; White-dense calcium; Dark Green-Fibrous; Light Green-Fibro-Fatty.

Table 1: List of patient information.

Patient	F1	F2	F3
Gender	Male	Male	Male
Age	52	71	68
Systolic Pressure(mmHg)	135	125	120
Diastolic Pressure(mmHg)	60	70	70
Smoke	Yes	No	No
Diagnosis History	Stable Angina	None	Stable Angina

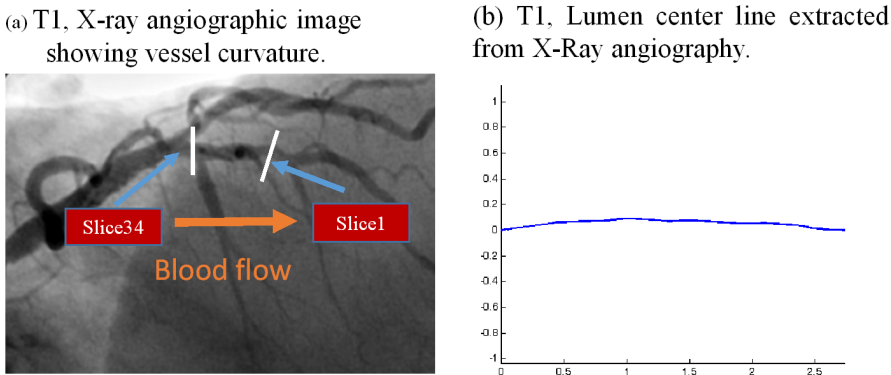


Figure 2: X-Ray angiographic image and extracted centerlines of the coronary segment.

2.2 *Plaque geometry reconstruction*

The arteries are axially stretched and pressurized under physiological conditions. Therefore, it is necessary to shrink the in vivo data to obtain an approximate computational starting shape so that the vessel could recover its in vivo geometry after pressurization and axial stretch. For 2D structure-only and 3D FSI models based on in vivo image data, a patient-specific shrinking process needs to be employed to deal with segmented plaque contour to obtain the no-load starting geometry for computational simulations [17, 18]. Figure 3 presented the shrinkage process of one 2D model and also presented the stress comparison of two models (one with shrink and the other without shrink) showing the importance of shrinkage process in calculating mechanical stress values. In addition, coronary arteries are subjected to cyclic bending caused by heart contraction/expansion. This has to be included in 3D coronary models for accurate computational predictions. The most time-consuming part in model construction is 3D mesh generation. All the segmented contour data were put into ADINA to reconstruct the 3D vessel geometry with finite element mesh using the procedures described in Yang et al. [15].

2.3 *The computational model and solution method*

The vessel material was assumed to be hyperelastic, anisotropic, nearly-incompressible and homogeneous. Plaque components were assumed to be hyperelastic, isotropic, nearly-incompressible and homogeneous for simplicity. No-slip conditions and natural traction equilibrium conditions were assumed at all interfaces. Our complete FSI model can be found from Yang et al. and are omitted here [15].

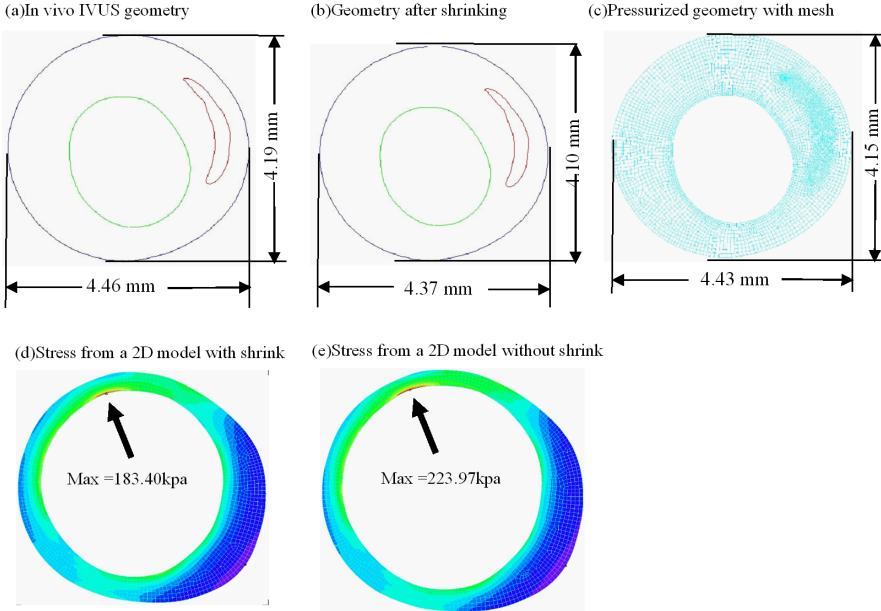


Figure 3: Plots of contours of a 2D slice with and without pre-shrink process and their corresponding plaque wall stress distributions showing the impact of the pre-shrink process.

Biaxial testing was performed using eight coronary arteries from 4 cadavers (age: 50-81) to obtain realistic vessel material data for our model [19]. A modified Mooney-Rivlin model was used for the vessel fitting our biaxial data: [15,19]

$$W = c_1(I_1 - 3) + c_2(I_2 - 3) + D_1[\exp(D_2(I_1 - 3)) - 1] + K_1/2K_2\{\exp[K_2(I_4 - 1)^2 - 1]\}. \quad (1)$$

$$I_1 = \sum C_{ii}, \quad I_2 = 1/2[I_1^2 - C_{ij}C_{ij}], \quad (2)$$

where I_1 and I_2 are the first and second invariants of right Cauchy-Green deformation tensor \mathbf{C} defined as $\mathbf{C} = [C_{ij}] = \mathbf{X}^T \mathbf{X}$, $\mathbf{X} = [X_{ij}] = [\partial x_i / \partial a_j]$, (x_i) is current position, (a_i) is original position, $I_4 = C_{ij}(\mathbf{n}_c)_i(\mathbf{n}_c)_j$, \mathbf{n}_c is the unit vector in the circumferential direction of the vessel, c_1 , D_1 , D_2 , and K_1 and K_2 are material constants. The parameter values used in this paper were:

$c_1 = -1312.9$ kPa, $c_2 = 114.7$ kPa, $D_1 = 629.7$ kPa, $D_2 = 2.0$, $K_1 = 35.9$ kPa, $K_2 = 23.5$. Our measurements are also consistent with data available in the literature [2, 13, 20, 21].

For 2D structure-only models, a single data set of blood pressure waveform, which was scaled according to the diastolic and systolic pressures of each patient, was used to apply over the lumen contour. Figure 4 presented a typical pressure waveform used in a model. In our FSI model with cyclic bending, blood flow was assumed to be laminar, Newtonian, and incompressible. The Navier-Stokes equations with arbitrary Lagrangian-Eulerian formulation were used as the governing equations. Pulsating pressure conditions were specified at the inlet and outlet using patient's systole and diastole arm pressure conditions. Cyclic bending was specified by prescribing periodic displacement at the myocardium side of the vessel using data obtained from X-Ray angiography.

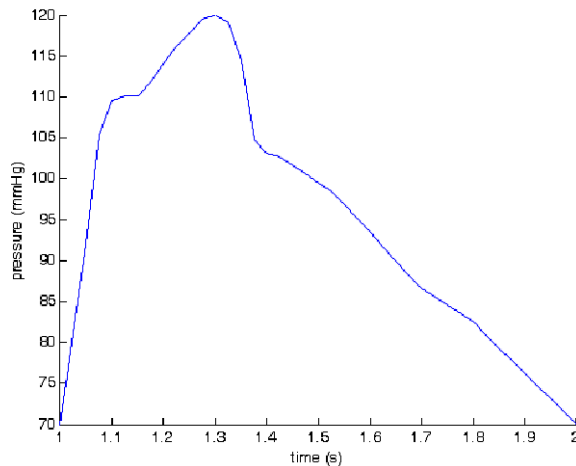


Figure 4: Sketch of a typical pressure profile.

The computational models were solved using the commercial finite package ADINA (ADINA R&D Inc., USA). Mesh analysis was performed by decreasing mesh size by 10% (in each dimension) until solution differences (measured by L2 norms of solution differences of all mechanical factors, including stress, strain, displacements and pressure) were less than 2%. Simulation for each plaque was run for 3 periods and the third period was almost identical to the second period and was then taken as the solution. More details of the computational models and solution methods can be found in Tang et al. [2].

2.4 Data extraction for correlation analysis

For each patient, IVUS slices at baseline (Time 1, T1) and follow-up (Time 2, T2) were matched up using vessel bifurcation, stenosis features and with careful review

by the IVUS group. For each slice, 100 evenly-spaced nodal points were selected on the lumen; each lumen nodal point was connected to a corresponding point on vessel out-boundary. Each slice was divided into 4 quarters for data analysis (see Figure 5). Vessel wall thickness (WT), PWS and PWSn values from 2D structure-only/3D FSI model solutions at each point were recorded for statistical analysis. Plaque progression was measured by wall thickness increase (WTI) from baseline to follow-up.

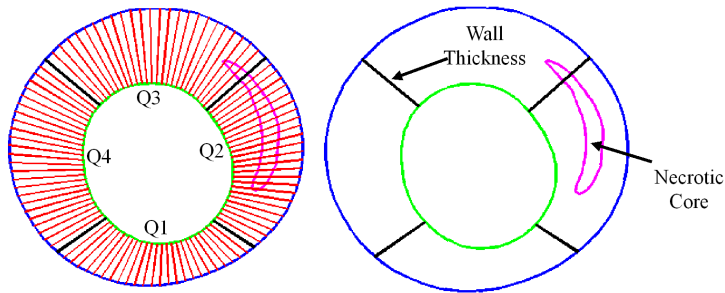


Figure 5: Sketch explaining definitions of quarters and wall thickness.

2.5 Statistical analysis

Pearson correlation coefficient was used for all correlation analysis. Correlations with $p < 0.05$ were deemed significant. When comparing the result differences between 2D structure-only and 3D FSI models, the following formula was used to calculate the error between the results in 2D structure-only and 3D FSI models.

$$Error = \sum_{i=1}^n |a_i - b_i| / \sum_{i=1}^n |b_i| \tag{3}$$

where a_i is the value of a given quantity corresponding to a node in 2D structure-only models and b_i is the value corresponding to the same node in FSI models, n is the total number of nodes of all slices in a whole patient model.

3 Results

3.1 Comparing 2D and 3D Models using wall thickness, stress and strain

Table 2 summarized the differences and correlation of wall thickness (WT), plaque wall stress (PWS) and plaque wall strain (PWSn) between 2D structure-only and 3D FSI models calculated by using the lumen node value of all 127 paired slices. It

can be seen that slice geometry of 2D models matched 3D geometry with individual case error ranging from 3.9% to 7.4% and overall error 5.4%. Overall 2D and 3D PWS and PWSn differed by 30% and 33%, respectively. Differences for individual plaques (6 plaques total) from 17% and 42%. However, 2D WT correlated strong positively with 3D WT. 2D PWS had positive correlation with 3D PWS, slightly weaker compared to that of WT. And 2D PWSn also correlated positively with 3D PWSn, much slightly weaker, compared to that of WT. Figure 6 gave a comparison of stress and strain between 2D and 3D models using one slice.

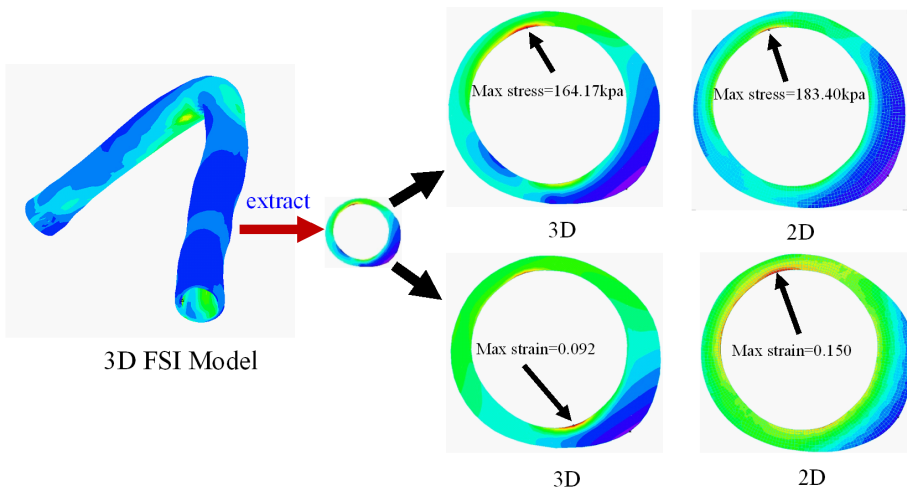


Figure 6: Plots showing 2D models over-estimated plaque stress and strain, compared to 3D model results.

3.2 2D/3D correlation results between plaque progression (WTI) and wall thickness (WT) agree well

Treating each slice as a case, Table 3 gives 3D correlation results between wall thickness increase (WTI) and three risk factors: WT, PWS and PWSn at Time 1 and summary of 2D agreement cases (n=127). The number of slices showing WTI correlated negatively with WT at T1 is larger than the other two situations (three patients together: negative correlation: 94 slices, Positive correlation: 21 slices, No significance correlation: 12 slices). Combining 2D and 3D models correlation between WTI and WT, overall 116 (91.3%) out of 127 slices have consistent correlation results between WTI and WT at T1.

Table 2: Comparison of wall thickness (WT), plaque wall stress (PWS) and plaque wall strain (PWSn) between 2D structure-only and 3D FSI models.

		WT				
Case	Nodes	2D	3D	error	r	p
P1	5700	0.47(0.18)	0.45(0.18)	4.4%	0.994	< 0.0001
P2	5700	0.46(0.21)	0.44(0.21)	6.2%	0.990	< 0.0001
P3	3600	0.70(0.34)	0.70(0.34)	3.9%	0.994	< 0.0001
P4	3600	0.77(0.39)	0.74(0.39)	4.4%	0.998	< 0.0001
P5	3400	0.81(0.34)	0.76(0.33)	7.4%	0.985	< 0.0001
P6	3400	0.80(0.24)	0.76(0.23)	6.1%	0.972	< 0.0001
All	25400	0.63(0.32)	0.61(0.31)	5.4%	0.992	< 0.0001
		PWS				
Case	Nodes	2D	3D	error	r	p
P1	5700	95.8(45.7)	70.9(32.6)	42%	0.747	< 0.0001
P2	5700	91.0(40.6)	70.6(34.3)	36%	0.780	< 0.0001
P3	3600	81.3(47.6)	76.5(46.6)	24%	0.846	< 0.0001
P4	3600	76.3(46.6)	69.1(44.3)	20%	0.902	< 0.0001
P5	3400	88.5(51.4)	92.9(53.4)	17%	0.923	< 0.0001
P6	3400	62.2(34.3)	69.3(34.6)	33%	0.639	< 0.0001
All	25400	84.4(45.8)	74.1(41.1)	30%	0.786	< 0.0001
		PWSn				
Case	Nodes	2D	3D	error	r	p
P1	5700	0.10(0.02)	0.07(0.02)	38%	0.662	< 0.0001
P2	5700	0.10(0.02)	0.07(0.02)	35%	0.639	< 0.0001
P3	3600	0.09(0.03)	0.07(0.02)	34%	0.554	< 0.0001
P4	3600	0.09(0.02)	0.06(0.02)	41%	0.816	< 0.0001
P5	3400	0.08(0.04)	0.07(0.03)	18%	0.804	< 0.0001
P6	3400	0.06(0.02)	0.07(0.02)	26%	0.451	0.0028
All	25400	0.09(0.03)	0.07(0.02)	33%	0.606	< 0.0001

3.3 Correlation between plaque progression (WTI) and PWS using slices, 2D and 3D comparisons

3D models correlation results between WTI and PWS at baseline (T1) is also presented in Table 3. The (Positive : Negative : No Significance) correlation ratio was (96:10:21). Comparing 2D and 3D models, 103 (81.1%) out of 127 slices had consistent correlation results.

3.4 Correlation between plaque progression (WTI) and PWSn using slices, 2D and 3D comparisons

Table 3 shows the (Positive : Negative : No Significance) correlation ratio was (92:14:21). Comparing 2D and 3D models, 99 (78%) out of 127 slices had consistent correlation results.

Table 3: 3D correlation results between wall thickness increase (WTI) and three risk factors: WT, PWS and PWSn at Time 1 and summary of 2D model correlation agreements with 3D models using 127 paired slices.

3D Correlation Results					All Cases 2D/3D Comparison
Patient	# of Slices	Positive	Negative	No signifi- cance	
WTI VS. WT at T1, 3D Correlations					2D Agreement
F1	57	20	27	10	48
F2	36	0	36	0	36
F3	34	1	31	2	32
Total	127	21	94	12	116 (91.3%)
WTI VS. PWS at T1					2D Agreement
F1	57	32	10	15	39
F2	36	33	0	3	32
F3	34	31	0	3	32
Total	127	96	10	21	103 (81.1%)
WTI VS. PWSn at T1					2D Agreement
F1	57	42	9	6	44
F2	36	25	1	10	28
F3	34	25	4	5	27
Total	127	92	14	21	99 (78%)

3.5 Correlation between plaque progression (WTI) and wall thickness (WT), PWS, PWSn, 2D and 3D comparison using quarters at patient level

Correlation between wall thickness increase (WTI) and risk factors including wall thickness (WT), plaque wall stress (PWS) and plaque wall strain (PWSn) predicted by 2D and 3D models using quarter average values are given by Table 4. For the three risk factors considered, the “all-quarters-combined” correlation results for 2D and 3D models were in agreement. Considering each patient as an individual, we have 3×3 correlation cases. 2D and 3D results were in agreement for all the 9

cases. Seven out of 9 had significant correlation predictions, while the other 2 had “no-significance” correlations.

Table 4: 2D/3D comparisons of correlation results between wall thickness increase (WTI) and risk factors: WT, PWS, and PWSn at Time 1 using quarter average values showing 2D and 3D models provided similar correlation predictions.

WTI VS. WT at T1					
		2D Model		3D FSI Model	
Case	Qts	r	p	r	p
F1	228	-0.3845	< 0.0001	-0.4005	< 0.0001
F2	144	-0.3409	< 0.0001	-0.3422	< 0.0001
F3	136	-0.7276	< 0.0001	-0.7411	< 0.0001
All	508	-0.3802	< 0.0001	-0.3838	< 0.0001
WTI VS. PWS at T1					
Case	Qts	r	p	r	p
F1	228	0.3696	< 0.0001	0.3059	< 0.0001
F2	144	0.1742	0.0368	0.2245	0.0068
F3	136	0.0152	0.8608	0.0159	0.8544
All	508	0.1567	< 0.0001	0.1689	< 0.0001
WTI VS. PWSn at T1					
Case	Qts	r	p	r	p
F1	228	0.3963	< 0.0001	0.3836	< 0.0001
F2	144	0.0498	0.5535	0.1453	0.0823
F3	136	0.2128	0.0129	0.1772	0.0391
All	508	0.1562	< 0.0001	0.2042	< 0.0001

4 Discussion

While 3D vulnerable plaque models with fluid-structure interactions and cyclic bending represent better approximation to the biological reality, the cost of model construction limited their use in clinical applications. The study based on 127 paired slices showed that plaque progression analysis using 2D models had a good agreement with that of 3D FSI models, particularly for the correlation WTI VS. WT at T1 (116 out of 127 slices with agreement). Moreover, results from our plaque progression study based on 2D/3D models using quarters further indicated that 2D structure-only models could provide similar correlation results between plaque progression (WTI) and risk factors (WT, PWS and PWSn). Constructing a 2D model

takes only a few minutes while constructing a 3D FSI model takes several weeks for an experienced researcher which is impractical for clinical applications. This study added the possibility that 2D models could be developed into commercial products for clinical applications in the future.

Some limitations of this study include: a) exact match of slices was not possible because 3D models were subjected to axial stretch and responses to pressure load were different from 2D models; b) patient-specific and tissue-specific material properties were not available for our study; c) IVUS-VH cannot visualize thin caps: in fact, the lipid-rich core is often in 'contact' with the lumen. Since there is a commonly accepted 65 micron threshold value for cap thickness, we made cap with thickness about 50 micron when IVUS-VH data had lipid-rich core on the lumen; d) while the angiographic movie provided information for the position of the myocardium and partial information for curvature variations, two movies with different (preferably orthogonal) view angles are needed to re-construct the 3D motion of the coronary and provide accurate curvature variation information; e) some data such as zero-stress conditions (opening angle), multi-layer vessel morphology and material properties were not possible to measure non-invasively *in vivo*; f) interaction between the heart and vessel were not be included. A model coupling heart motion and coronary bending would be desirable when required data become available.

Acknowledgement: This work was supported in part by NIH grant NIH/NIBIB R01 EB004759. Chun Yang's research is supported in part by National Sciences Foundation of China 11171030.

References

1. Fleg, J. L., Stone, G. W., Fayad, Z. A., Granada, J. F., Hatsukami, T. S., Kolodgie, F. D., Ohayon, J., Pettigrew, R., Sabatine, M. S., Tearney, G. J., Waxman, S., Domanski, M. J., Srinivas, P. R. & Narula, J. (2012) Detection of high-risk atherosclerotic plaque: report of the NHLBI working group on current status and future directions. *JACC Cardio Imaging*, 5, 9, 941-55.
2. Tang, D., Kamm, R. D., Yang, C., Zheng, J., Canton, G., Bach, R., Huang, X., Hatsukami, T. S., Zhu, J., Ma, G., Maehara, A., Mintz, G. S. & Yuan, C. (2014) Image-based modeling for better understanding and assessment of atherosclerotic plaque progression and vulnerability: data, modeling, validation, uncertainty and predictions. *J. Biomech.*, 47, 4, 834-46.
3. Friedman, M. H., Krams, R. & Chandran, K. B. (2010) Flow interactions with cells and tissues: cardiovascular flows and fluid-structure interactions.

Ann. Biomed Eng., 38, 1178-1187.

4. Fuster, V. (1998) *The Vulnerable Atherosclerotic Plaque: Understanding, Identification, and Modification*, Editor: Valentin Fuster, Co-Editors: Cornhill, J. F., Dinsmore, R. E., Fallon, J. T., Insull, W., Libby, P., Nissen, S., Rosenfeld, M. E., Wagner, W. D., AHA Monograph series, Futura Publishing, Armonk NY.
5. Ku, D. N., Giddens, D. P., Zarins, C. K. & Glagov, S. (1985) Pulsatile flow and atherosclerosis in the human carotid bifurcation: positive correlation between plaque location and low and oscillating shear stress. *Arteriosclerosis*, 5, 293-302.
6. Richardson, P. D. (2002) Biomechanics of plaque rupture: progress, problems, and new frontiers. *Ann Biomed Eng.*, 30, 4, 524-36.
7. Underhill, H. R., Hatsukami, T. S., Fayad, Z. A., Fuster, V. & Yuan, C. (2010) MRI of carotid atherosclerosis: clinical implications and future directions. *Nature Reviews Cardiology*, 7, 1, 165-173.
8. Tang, D., Yang, C., Mondal, S., Liu, F., Canton, G., Hatsukami, T. S. & Yuan, C. (2008) A negative correlation between human carotid atherosclerotic plaque progression and plaque wall stress: *in vivo* MRI-based 2D/3D FSI models. *J. Biomech.*, 41, 4, 727-736.
9. Stone, P. H., Saito, S., Takahashi, S., Makita, Y., Nakamura, S., Kawasaki, T., Takahashi, A., Katsuki, T., Nakamura, S., Namiki, A., Hirohata, A., Matsumura, T., Yamazaki, S., Yokoi, H., Tanaka, S. Otsuji, S., Yoshimachi, F., Honye, J., Harwood, D., Reitman, M., Coskun, A. U., Papafaklis, M. I. & Feldman, C. L. (2012) Prediction of progression of coronary artery disease and clinical outcomes using vascular profiling of endothelial shear stress and arterial plaque characteristics: the PREDICTION Study. *Circulation*, 126, 2, 172-81.
10. Samady, H., Eshtehardi, P., McDaniel, M. C., Suo, J., Dhawan, S. S., Maynard, C., Timmins, L. H., Quyyumi, A. A. & Giddens, D. P. (2011) Coronary artery wall shear stress is associated with progression and transformation of atherosclerotic plaque and arterial remodeling in patients with coronary artery disease. *Circulation*, 124, 779-788.
11. Xie, Y., Mintz, G. S., Yang, J., Doi, H., Iñiguez, A., Dangas, G. D., Serruys, P. W., McPherson, J. A., Stone, B.G. W. & Maehara, A. (2014) Clinical out-

- come of nonculprit plaque ruptures in patients with acute coronary syndrome in the PROSPECT study. *JACC Cardiovasc Imaging*, 7, 4, 397-405.
12. Yang, C., Canton, G., Yuan, C., Ferguson, M., Hatsukami, T. S. & Tang, D. (2010) Advanced human carotid plaque progression correlates positively with flow shear stress: an in vivo MRI multi-patient 3D FSI study, *J. Biomechanics*, 43, 13, 2530-2538.
 13. Wang, L., Wu, Z., Yang, C., Zheng, J., Bach, R., Muccigrosso, D., Billiar, K., Maehara, A., Mintz, G. S. & Tang, D. (2015) IVUS-Based FSI Models for Human Coronary Plaque Progression Study: Components, Correlation and Predictive Analysis. *Annals of biomedical engineering*, 43, 1, 107-121.
 14. Huang, Y., Teng, Z., Sadat, U., Graves, M. J., Bennett, M. R. & Gillard, J. H. (2014) The influence of computational strategy on prediction of mechanical stress in carotid atherosclerotic plaques: comparison of 2D structure-only, 3D structure-only, one-way and fully coupled fluid-structure interaction analyses. *J. Biomech.*, 47, 6, 1465-71.
 15. Yang, C., Bach, R. G., Zheng, J., Naqa, I. E., Woodard, P. K., Teng, Z., Billiar, K. L., Tang, D. (2009) In vivo IVUS-based 3D fluid structure interaction models with cyclic bending and anisotropic vessel properties for human atherosclerotic coronary plaque mechanical analysis, *IEEE Trans. Biomed. Engineering*, 56, 10, 2420-2428.
 16. Wahle, A., Prause, P. M., DeJong, S. C. & Sonka, M. (1999) Geometrically correct 3-D reconstruction of intravascular ultrasound images by fusion with biplane angiography—methods and validation. *IEEE Trans Med Imaging*, 18, 8, 686-99.
 17. Tang, D., Teng, Z. Z., Canton, G., Yang, C., Ferguson, M., Huang, X., Zheng, J., Woodard, P. K. & Yuan, C. (2009) Sites of rupture in human atherosclerotic carotid plaques are associated with high structural stresses: an in vivo MRI-based 3D fluid-structure interaction study. *Stroke*, 40, 10, 3258-3263. Featured article on MDlinx.com.
 18. Tang, D., Teng, Z., Canton, G., Hatsukami, T. S., Dong, L., Huang, X. & Yuan, C. (2009) Local critical stress correlates better than global maximum stress with plaque morphological features linked to atherosclerotic plaque vulnerability: an in vivo multi-patient study. *Biomed. Eng. Online*, 8, 15, 1-9.

19. Kural, M. H., Cai, M. C., Tang, D., Gwyther, T., Zheng, J. & Billiar, K. L. (2012) Planar biaxial characterization of diseased human coronary and carotid arteries for computational modeling. *Journal of Biomech.* 45, 5, 790-798.
20. Holzapfel, G. A., Mulvihill, J. J., Cunnane, E. M. & Walsh, M. T. (2014). Computational approaches for analyzing the mechanics of atherosclerotic plaques: a review. *J. Biomech.* 47, 4, 859-69.
21. Holzapfel, G. A., Sommer, G., & Regitnig, P. (2004) Anisotropic mechanical properties of tissue components in human atherosclerotic plaques, *J. Biomech. Eng.*, 126, 5, 657-665.